



ARTICLE OPEN



Strategy to improve Cu-BTC metal-organic frameworks performance in removal of Rhodamine B: MD and WT-MtD simulations assessment

Leila Razavi¹, Heidar Raissi¹ , Hassan Hashemzadeh²  and Farzaneh Farzad¹

With industry progress, environmental problems have begun to threaten human health. Among them, water pollution is closely related to human life and has attracted researchers' attention. Hence, coping strategies for these pollutants have become a priority nowadays. Here, we carried out the molecular dynamics (MD) and well-tempered metadynamics simulations to evaluate the interaction of Rhodamine B (Rh B) with a copper (II)-benzene-1,3,5-tricarboxylate metal-organic framework (Cu-BTC/MOF). To design a more efficient dye removal platform, the effect of the -NH₂, -OH, and -NO₂ functional groups on the efficiency of Cu-BTC/MOF in the adsorption of Rh B is investigated. It is found that the interaction energy of Rh B with -NH₂-MOF, -OH-MOF, and -NO₂-MOF is about -79.98, -121.87, and -365.55 kJ mol⁻¹, respectively, more than the pristine case. This observation confirms that the functionalization strategy can enhance the Cu-BTC/MOF efficiency. The obtained free energy (FE) values from the metadynamics simulation indicated that for adsorption of Rh B on pristine, -NH₂-MOF, -OH-MOF, and -NO₂-MOF, the global minimums are located about at -220.47, -234.75, -236.09, and -259.01 kJ mol⁻¹, respectively. The obtained results show that in the two-dimensional FE surfaces, the most stable complex with Rh B belongs to the MOF-NO₂ system.

npj Clean Water (2022)5:47; <https://doi.org/10.1038/s41545-022-00195-w>

INTRODUCTION

With the development of industry, environmental problems have endangered human health, among which water pollution and its related problems have severe human life and health implications, therefore coping strategies for these pollutants has become a priority nowadays. Due to the rapid development of the application of the dyes industry, synthetic organic dyes pollution in water is known as the main source of environmental pollution^{1,2}.

Rhodamine B (Rh B) is a synthetic organic red dye with high solubility, extensively employed in the printing, textile industry, medicine for animals, etc. Rh B is dangerous to environmental, animal, and human health and can cause diverse health problems in humans, including respiratory tract, irritation to the skin, and degenerative changes in the kidney and liver. Hence, the removal of Rh B from wastewater has been widely concerned and researched^{3–5}.

Many strategies such as membrane filtration, photocatalysis, floatation, chemical oxidation and adsorption have been applied to remove harmful dye materials from wastewater. Among available techniques, adsorption due to its easy operation, simplicity, high efficiency, and low cost has been an extensively considered technique for the removal of dye^{6,7}. Different adsorbents such as graphene oxide (GOX), MXenes, and zeolite composites have been extensively employed for the removal of Rh B from wastewater samples^{8–10}. For instance, Narayanaswamy et al.¹¹ via molecular dynamics (MD) and Monte Carlo simulations examined the application of GOX and GOX-Fe₃O₄ as adsorbent materials for the removal of dye molecules. Their results demonstrated that the dyes are physisorbed on the adsorbent's surface through the formation of π - π stacking interaction. Furthermore, they showed the GOX-

Fe₃O₄ nanocomposite has a higher interlayer distance in comparison to the synthesized GOX, which helps in the removal of the higher amount of dyes.

Metal-organic frameworks (MOFs), consisting of organic ligands and metal ions, have a special structure with a large surface area and high porosity^{12–15}. The possibility to create a newly engineered combination by changing the organic ligand and metal ion make MOFs suitable candidates for different applications such as drug delivery^{16,17}, gas adsorption¹⁸, and gas separation¹⁹. Moreover, MOFs have been used in many different studies as effective adsorbents for sulfur compounds^{20,21}, phenols^{22,23}, and dyes^{17,24,25}. The most common ions for MOFs synthesis are copper, iron, manganese and zinc ions. Also, benzene-1,3,5-tricarboxylic acid (BTC) and 1H-1,2,4 triazole ligands are the common ligands for MOFs synthesis²⁶.

Functionalizing the organic part of the MOFs with different functional groups and having multiple active sites provide the possibility of achieving new compounds²⁷. Since the bulk shape of the MOFs can be an obstacle to their adsorption efficiency, hence, it is required to modify their morphology towards a more efficient environment for dye adsorption²⁸. Recently, Wu et al.¹ studied the Materials of the institute Lavoisier (MIL) for Rh B and tetracycline adsorption. Adsorption performance and mechanism were examined via kinetics, isotherms, and adsorption experiments. Their results demonstrated that the modified MIL has high potential as a practical adsorbent for the removal of aqueous Rh B and tetracycline.

It is well-known that the MD method can be utilized to study equilibrium, structure, and dynamic molecular properties of microscopic molecular systems based on the classic mechanical model of molecules²⁹. Molecular simulation is a powerful method in modern molecular modeling and enables us to

¹Department of Chemistry, University of Birjand, Birjand, Iran. ²Department of Pharmaceutics and Pharmaceutical Nanotechnology, School of Pharmacy, Birjand University of Medical Sciences, Birjand, Iran. ✉email: hraeisi@birjand.ac.ir

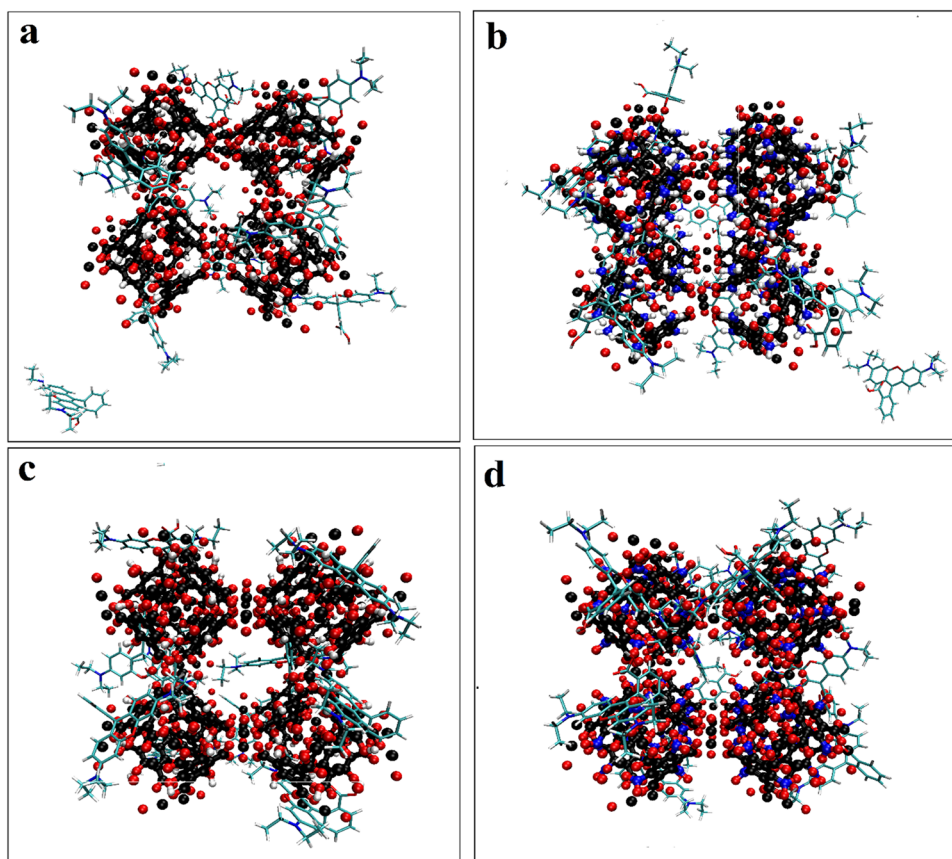


Fig. 1 Representative final configurations of studied systems after 75 ns of simulation. **a** MOF-Rh B, **b** MOF-NH₂, **c** MOF-OH and **d** MOF-NO₂ systems.

probe structure and dynamics with extreme detail on scales where the motion of individual atoms can be tracked. Also, the MD simulation is a helpful approach in terms of time-saving and cost-efficient for predicting the adsorption behavior of structures. Furthermore, MD simulations have been considered a suitable and powerful tool to explore atomic-level mechanisms which are usually out of the scope of current experimental tools³⁰.

The Well-tempered metadynamics (WT-MtD) simulation is an atomistic simulation technique that allows the estimation of the free energy (FE) of complex molecular systems. This method uses Gaussian-like bias to overcome high energy barriers on the FE surface. In WT-MtD, which is one of the types of metadynamics methods, the bias height of these Gaussians reduces over the simulation time. The WT-MtD simulation is also effective in describing the FE surface in terms of binding and unbinding^{31,32}.

Given the importance of Rh B removal as an important class of pollutants, this paper aims to the effectiveness of Cu-BTC/MOF in the Rh B adsorption is accomplished using the MD and WT-MtD simulations. Then, the adsorbent is functionalized with amino, hydroxyl, and nitro groups, and their efficiencies are examined and compared. The studies on MOFs are primarily concentrated on gas adsorption and very few reports can be found studying dyes adsorption to date³³. Also, the adsorption of Rh B dye and the effect of different functional groups on the Cu-BTC/MOF (F-MOF) surface via MD and WT-MtD simulations have not been investigated. Therefore, this contemplated us employing Cu-BTC/MOF to study the adsorption of Rh B dye. This work provides

valuable information on the adsorption mechanism of Rh B on the surfaces of Cu-BTC/MOF and F-MOF.

RESULTS AND DISCUSSION

Md simulation

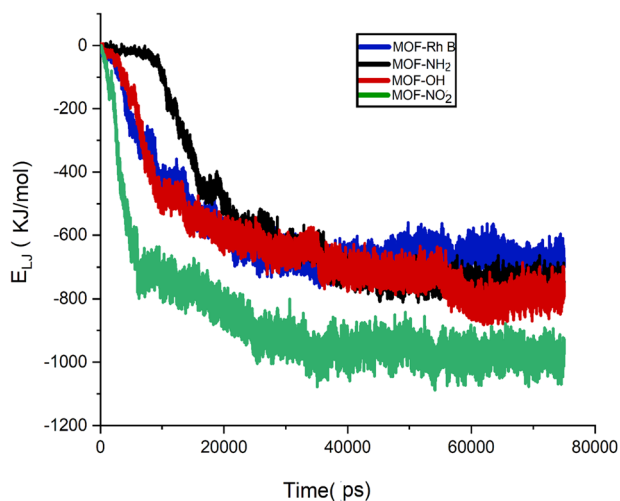
There are several research works that shown the Cu-BTC/MOF has much higher dye removal efficiency in comparison to the other adsorbents^{11,34,35}. As well as, Naqi Ahamad and co-workers observed that the dye removal capacity of MOF is affected by the functional group³⁶. Therefore, in this section, the adsorption behavior of Rh B molecules on Cu-BTC/MOF and F-MOFs is studied. Snapshots of the configuration of dye-MOF complexes at two different times (i.e., 20 and 75 ns) are depicted in Supplementary Fig. 1.

As shown in these Figures, after ~20 ns of MD simulations, the dye molecules moved to adopt a more parallel conformation. In this position, they can form the hydrogen bond (H-bond) and π - π interaction with adsorbent surface. In MOF-OH and MOF-NO₂ systems, all Rh B molecules are adsorbed on the adsorbent surface, while in the other two systems, one Rh B molecule is located further far away from the adsorbent surfaces (See Fig. 1). It is known that Rh B, through its three benzene rings, forms strong π - π stacking interactions with the adsorbent surface. Besides, the X-H... π (X:O, N, and C) intermolecular interactions between Rhodamine B and the adsorbent surfaces are also observed. The C-H... π , N-H... π and O-H... π intermolecular interactions between Rh B and adsorbents occur at a distance of ~0.25–0.39 nm. Also, it was found that the functionalization of Cu-BTC/MOF improves the capacity of the adsorbent to adsorb the Rh B. MOFs-Rh B Lennard-

Table 1. The LJ, Coul, and Tot energies between of Rh B and adsorbent in the Cu-CTC/MOF and F-MOF systems.

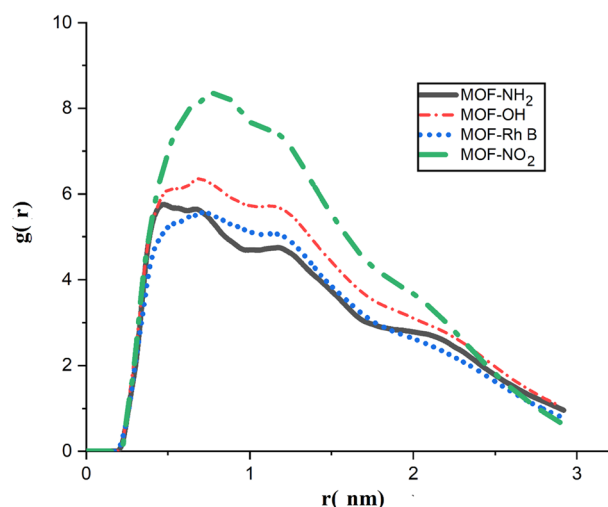
Systems	LJ	Coul	Tot
MOF-Rh B	-504.02	-1.59	-502.43
MOF-NH ₂	-584.01	-9.97	-574.04
MOF-OH	-625.90	-14.81	-611.09
MOF-NO ₂	-869.79	-21.06	-848.73

(All energy values in kJ mol⁻¹).

**Fig. 2** Interaction energy of the dye molecules with MOF (blue), MOF-NH₂ (black), MOF-OH (red), and MOF-NO₂ (green) as a function of simulation time.

Jones (L-J), coulombic (Coul), and Total (Tot = L-J + Coul) energy values are calculated, and the precise numerical values are listed in Table 1. From the data presented in this Table, it is evident that the Elec interaction energy is much less than L-J energy because the surface charge of adsorbents is almost neutral. Therefore, interaction energy is mainly provided by L-J energy, even though the functional groups added on Cu-BTC/MOF improved the coulombic energy of the systems. The comparison of the adsorption energy values in this work with previous works (See Supplementary Table 1) shows that the interaction of Rh B with Cu-BTC/MOF is stronger than the other adsorbents, which confirms that Cu-BTC/MOF has good potential for the removal of Rh B.

The L-J interactions between atoms and molecules are ubiquitous and significant for many molecular and condensed-matter structures³⁷. At the beginning of the simulation, Rh B is placed at a distance of ~2 nm from the adsorbent surface so that the L-J interaction energy is set to zero. Figure 2 shows the L-J energy between Rh B molecules and MOFs as a function of simulation time. As seen in this figure, Rh B molecules are adsorbed on MOFs quickly after ~20 ns, and their pair interaction fluctuates around its average value (~-700 kJ mol⁻¹) for the rest of the simulation time. It is worth noting that after the adsorption of Rh B on the adsorbent surfaces, the Lennard-Jones interaction energy decreases, then the L-J interaction energy value almost becomes a constant. In the MOF-NO₂ system, ~90% of Rh B molecules are adsorbed on the adsorbent surface at the initial 30 ns. From 30 to 75 ns, all of Rh B molecules (cf. 100%) are adsorbed, which shows that the capacity of the -NO₂-MOF is better compared to the adsorbent used in the work of Dadashi Firouzjaei group (GOX-Cu-BTC/MOF)¹⁷. As well as, the obtained

**Fig. 3** The RDF of Rh B molecules with respect to the MOF (blue), MOF-NH₂ (black), MOF-OH (red), and MOFNO₂ (green).

results showed that the interaction energy value in the MOF-Rh B system is about -500 kJ mol⁻¹. These findings are in good agreement with the recent computational and experimental results reported by Dadashi Firouzjaei and co-workers¹⁷. As you can see in Fig. 2 the energy-decreasing trend becomes more intense in the MOF-NO₂ system, and the L-J energy decreases more than in the other systems, which shows that Rh B tends to make stronger interactions with the -NO₂-MOF. This fact can be attributed to the presence of the strong electron-withdrawing group (-NO₂) and more dye adsorption in this system. Furthermore, the -OH-MOF and -NH₂-MOF show better performance than Cu-BTC/MOF in the adsorption of Rh B. This observation confirmed that the presence of additive molecules led to the reinforcement of the interactions of Rh B with the adsorbent that showed by Naqi Ahamad and co-workers³⁶.

The Radial distribution function (RDF) is analyzed from the MD simulation for acquiring a better understanding of the stability of MOF/dye and F-MOF/dye systems in water solution. The RDF is defined as the probability of locating particle "j" within the range (r + dr) of particle i which is usually denoted as g(r)^{38,39}. Figure 3 represents the RDFs obtained between the COM of adsorbent and Rh B molecules in the simulation systems.

As it is obvious from this Figure, the main interactions between Rh B and adsorbents exist at a distance of about 0.3–1.5 nm, and the maximum interactions occur at 0.7 nm. The strongest RDF peaks between Rh B and adsorbents can be observed in the MOF-NO₂ and MOF-OH systems at distances of approximately 0.63 and 0.7 nm. This observation reveals that in these two systems, the probability of finding Rh B is higher both in terms of closeness to the surface and amount. This conclusion is consistent with the fact that the L-J energy in these systems is higher than in the MOF-Rh B and MOF-NH₂ systems. Also, the sharper peak for these two systems indicates the strong interaction of Rh B with the adsorbent adsorption sites.

Atomic RDFs (aRDFs) are provided to describe how the atomic density varies as a function of the distance from one special atom of the reference molecule³⁹. The RDF of various atoms of the nearest Rh B molecule around the adsorbent surface is shown in Fig. 4. As it is obvious from Fig. 4a, the interaction of O_{Rh B} - C_{Cu-BTC/MOF} depicted an intense peak at around 0.71 nm. The highest O_{Rh B} - C_{adsorbent} peak belonged to the MOF-NO₂ system, where the L-J interaction is much higher than that in the other systems (ref. Fig. 2). The same trend is observed for the intensity of the O_{Rh B} - C_{adsorbent} peak and L-J energy for other systems. Also, the sharp peak of the H_{Rh B} - C_{adsorbent} RDFs confirms the strong

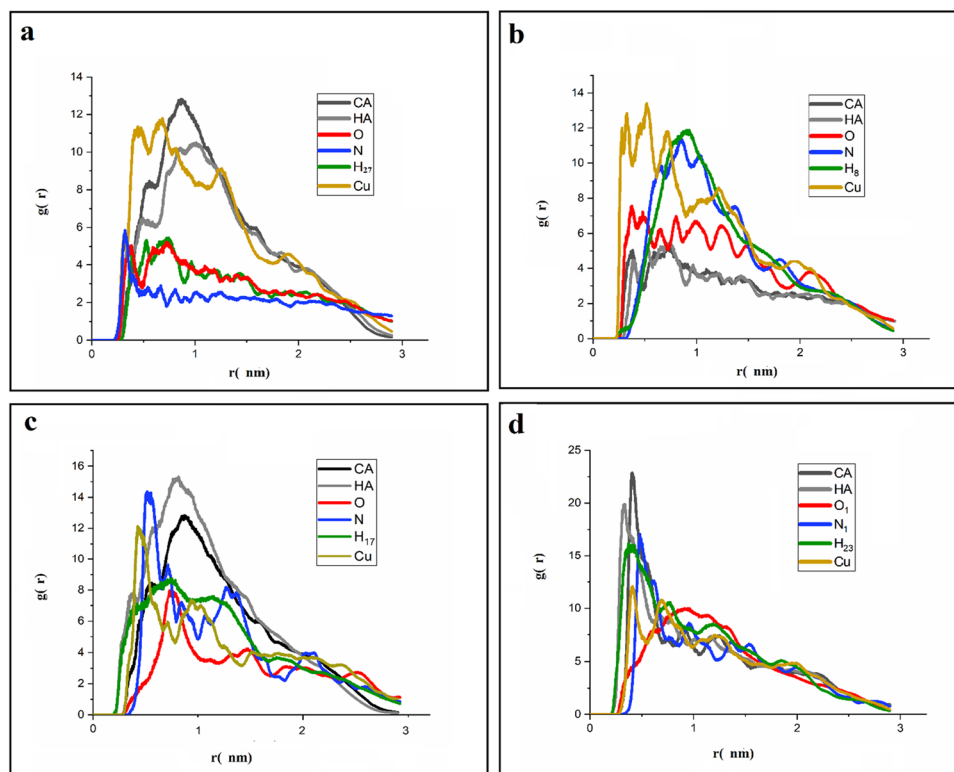


Fig. 4 The atomic RDF patterns. **a** MOF-Rh B, **b** MOF-NH₂, **c** MOF-OH and **d** MOF-NO₂ systems.

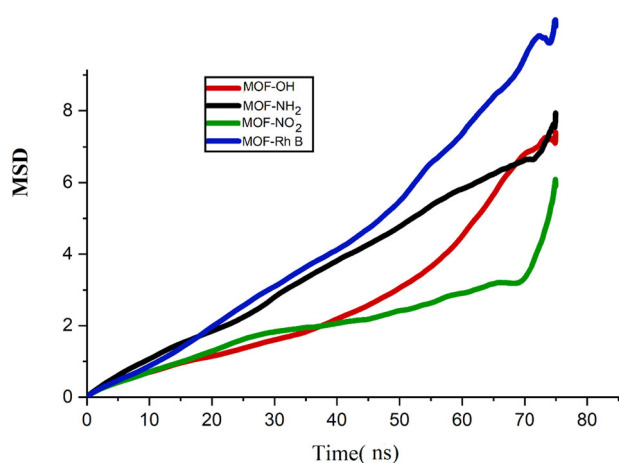


Fig. 5 Time evolutions of MSD of Rh B at the MOF (blue), MOF-NH₂ (black), MOF-OH (red), and MOF-NO₂ (green) systems.

H-bond interaction between dye and adsorbents at a distance of ~ 0.7 – 0.8 nm in MOF-NH₂ and MOF-OH systems. As seen in this figure, the sharp peaks of the HA and CA atoms (aromatic ring atoms) are located at 0.3–1.4 nm. These results corroborate that the π - π stacking between Rh B and the Cu-BTC/MOF and F-MOFs surfaces plays the main role in dye adsorption. Close inspection of Fig. 4 confirms that Rh B's nitrogen atom in the MOF-NO₂ system has a higher propensity for interaction with -NO₂-MOF cavities in contrast to other systems. In addition, Fig. 4 shows strong RDF peaks for copper atoms, especially in the MOF-OH and MOF-NO₂ systems. This fact can be related to the location of Cu atoms in Cu-BTC/MOF which, is placed close to the internal region of MOF's cavity; thus, dye molecules are naturally located close to the copper atoms.

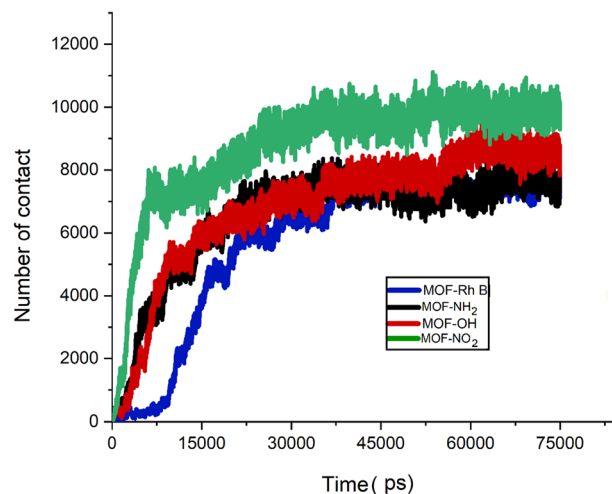


Fig. 6 The variations of the number of contacts between the guest molecules and the MOF (blue), MOF-NH₂ (black), MOF-OH (red), and MOF-NO₂ (green) surface.

The mean-square displacement (MSD) and self-diffusion coefficient (D_i) are considered to estimate the mobility of a molecule^{40,41}. The diffusion of Rh B molecules to the adsorbent surface, which is calculated from the MSD curve slope, can be used for the evaluation of the interactions between dye molecules and MOFs (Fig. 5).

The smaller slope in the MSD curves of dye molecules in the MOF-NO₂ system represents that the adsorption of Rh B on the adsorbent surface restricts dye movement. This observation can be ascribed to the effect of the NO₂ functional group in the adsorption of Rh B on the adsorbent surface. These trends emphasize that in the MOF-NO₂ and MOF-OH systems the adsorption of dye molecules into the cavities of the adsorbent is

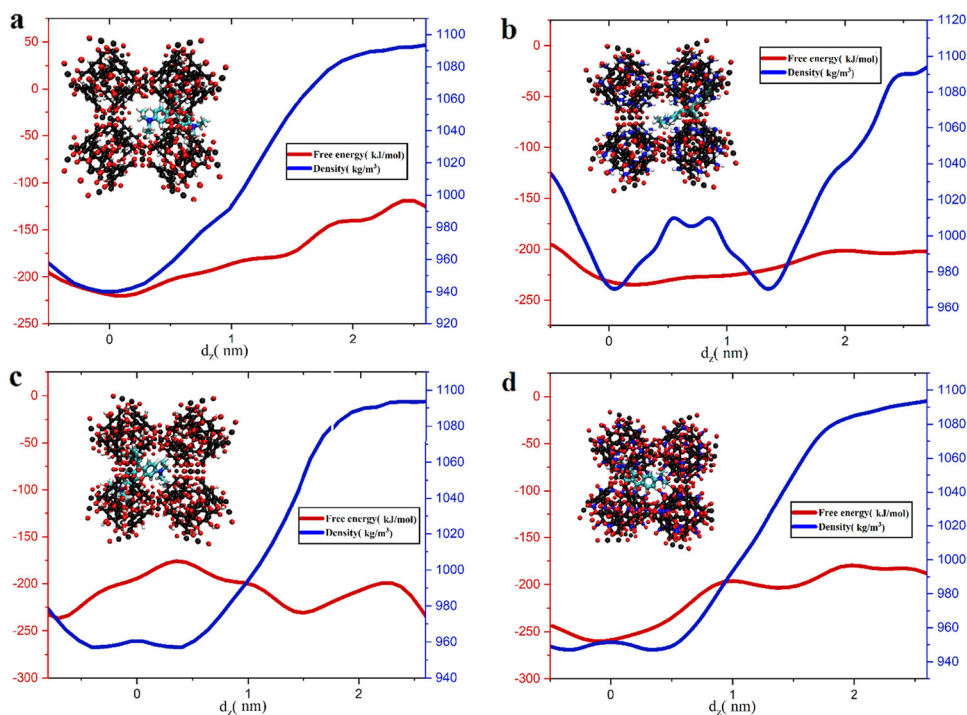


Fig. 7 The water density profile and FE landscape. For the adsorption of Rh B on **a** the Cu-BTC/MOF (MOF-Rh B system) and F-MOF surfaces **b** MOF-NH₂ system, **c** MOF-OH system and **d** MOF-NO₂ system as a function of their center of masses.

preferable with respect to MOF-Rh B and MOF-NH₂. The Diffusion coefficient (D_i) is evaluated by Supplementary Eq. 1⁴² and has been tabulated in Supplementary Table 2. Based on the results in this Table, in the MOF-Rh B system, Rh B molecules showed higher D_i and error values compared with other systems. This finding can be related to its weaker interaction of Rh B with Cu-BTC/MOF. This is confirmed by the RDF results in Fig. 3, which show that the distance between Rh B and the adsorbent is shorter than in the other three systems. On the other hand, the lower D_i values for MOF-OH and MOF-NH₂ systems are due to the strong interaction of Rh B with adsorbent adsorption sites. The small D_i value for the MOF-NH₂ system can be attributed to the more dye-adsorbent collisions and the strong blocking effect of the functional groups.

To further justify the above findings, we have computed the number of contacts between Rh B and adsorbents and have plotted those as a function of simulation time in Fig. 6. As seen in this figure, at 0 ns there is no contact between Rh B and the adsorbent. During the simulation time, the number of contacts increases by adsorbing Rh B on the adsorbents. The atomic contact number is observed to reach highest in the MOF-NO₂ system strength. This result indicates the strong interaction of Rh B with the -NO₂-MOF and -OH-MOF adsorption sites. For the MOF-OH and the MOF-NH₂ systems, the number of contacts decreased, and the lowest values are recorded for the MOF-Rh B system. In accordance with other obtained results in this study, the reduced number of contacts in the MOF-Rh B system confirms that the Rh B is weakly adsorbed on Cu-BTC/MOF.

Metadynamics

Exploration of FE surface for all four systems containing an adsorbent, functional group, and Rh B is investigated through WT-MtD simulations, and the results are depicted in Fig. 7. This Figure demonstrates the FE surface as a function of the distance between the Rh B's COM and the adsorbents. In the investigated systems, the FE of Rh B can vary as a function of its position (in the water phase, at the water-adsorbent interface, on the adsorbent surface). In the water phase, the FE profile of the MOFs-Rh B systems is

more than -120 kJ mol^{-1} . In the MOF-Rh B system, the FE is decreased as the dye molecule moves from the water phase toward the adsorbent cavities. Moreover, the dye molecule is encountered with a relatively small energy barrier ($\sim 4 \text{ kJ mol}^{-1}$) when it reaches the water-adsorbent interface. By crossing this barrier, while the dye molecule approaches the adsorbent cavities, the decrease in FE value is continued to achieve the most stable state. As shown in Fig. 7a, this point is 0.2 nm away from the adsorbent, and its energy is $\sim -220.47 \text{ kJ mol}^{-1}$. The FE in the MOF-NH₂ system illustrates the same trend as the MOF-Rh B system because, in both systems, the dye must overcome a small energy barrier ($\sim 4 \text{ kJ mol}^{-1}$) to achieve the MOF-NH₂ and water interface. Nonetheless, Rh B does not encounter any energy barrier to adsorption on the MOF-NH₂ surface and eventually reaches a minimum point with an energy of $-234.75 \text{ kJ mol}^{-1}$. In the MOF-OH system, Rh B should pass an energy barrier of $\sim 55 \text{ kJ mol}^{-1}$ to transfer from the water phase to the interface. After passing this barrier, the EF surface reveals a global minimum ($\sim -236.09 \text{ kJ mol}^{-1}$) for the interaction of Rh B and the MOF-NH₂. The FE for the MOF-NO₂ system shows that the dye molecule faces two small energy barriers (about 4 and 6 kJ mol^{-1}) to reach the water-adsorbent interface. From Fig. 7b–d panels, it is evident that in the MOF-NH₂ and MOF-OH systems, the FE value is almost identical, while in system MOF-NO₂, the value of FE is increased. The two-dimensional FE surface as a function of the chosen CV of adsorbents/Rh B and functional groups/Rh B is shown in Fig. 8. In this figure, it can be observed that Rh B shows a global minimum where the $CV_{\text{Cu-BTC/MOF_Rh B}}$ and $CV_{\text{NO}_2\text{Rh B}}$ are small. At this point, both adsorbent and NO₂ group components have efficient involvement in the adsorption of the dye molecule that for achieving this point, Rh B almost does not face any high-energy barrier. Close inspection of Fig. 8b, confirms that the interaction distance of OH group and Rh B is smaller than Cu-BTC/MOF_Rh B. This can be related to nature of the OH group-dye interaction, where the H-bond is the main intermolecular interaction. Based on the derived 3D landscape, The lowest value of FE $-186.5 \text{ kJ mol}^{-1}$ is calculated in the coordinates $d_1 = 0.3 \text{ nm}$ and $d_2 = 2.01 \text{ nm}$ (Fig.

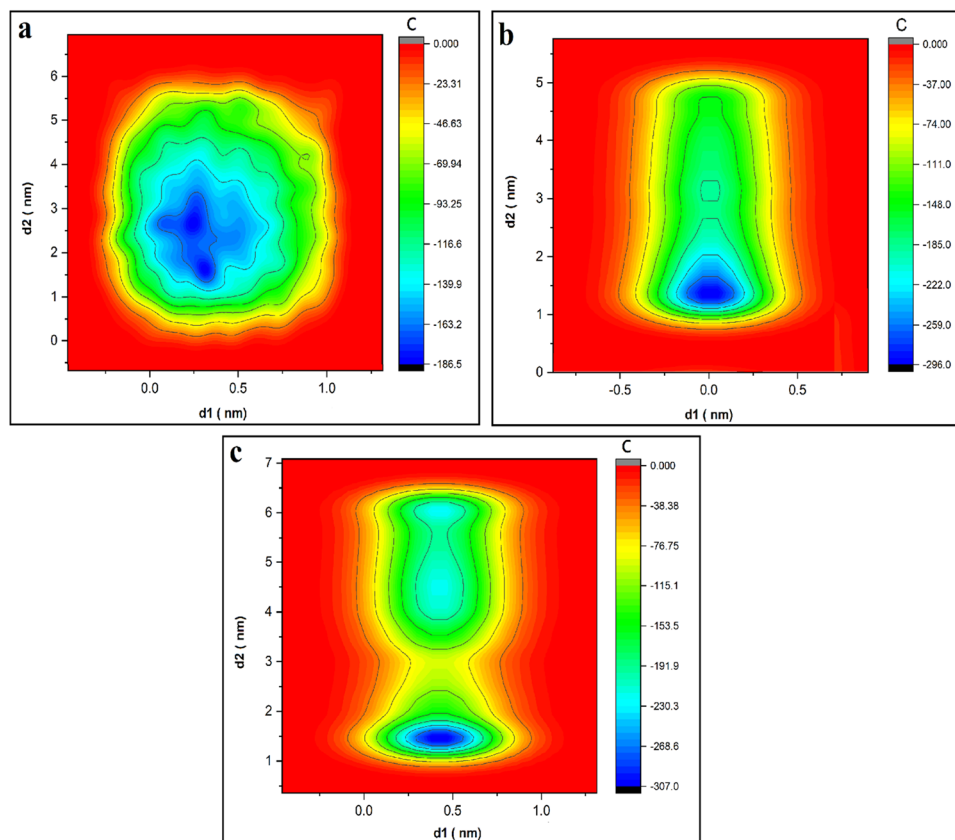


Fig. 8 FE landscape as a function of $d1$ and $d2$, which are the distance of the Rh B COM from the Cu-BTC/MOF COM and functional groups, respectively. **a** MOF-NH₂, **b** MOF-OH, and **c** MOF-NO₂ systems.

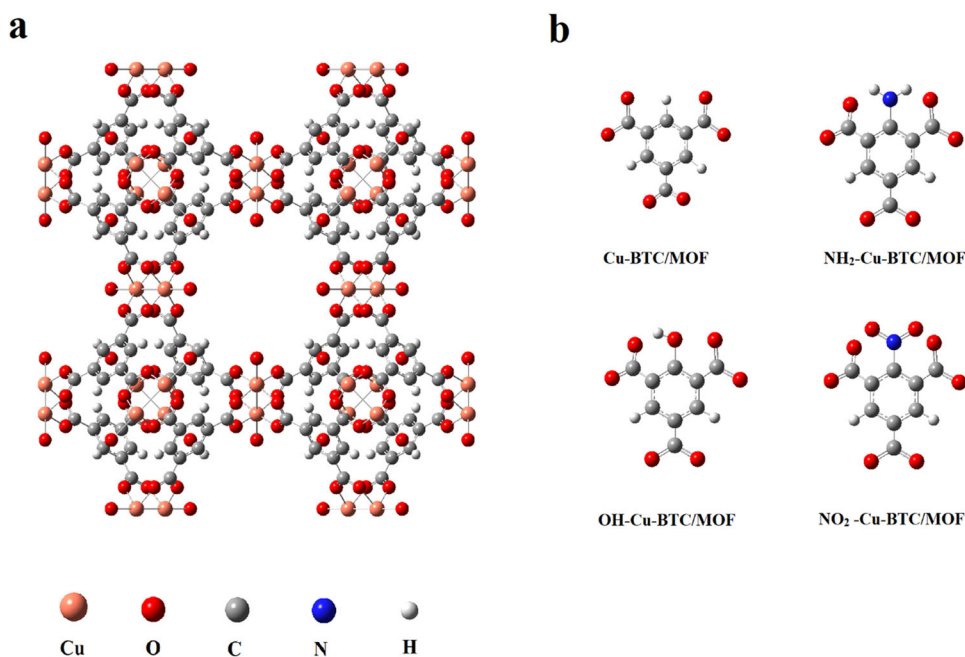


Fig. 9 Structure of **a** Cu-BTC/MOF and **b** Functionalized organic linker parts.

8a). In agreement with MD simulation, the metadynamics simulation results also confirmed a reduction in FE of the global minimum in the above-mentioned systems. In agreement with MD simulation, the WT-MtD simulation results also confirmed a reduction in FE of the global minimum in the studied systems. All

in all, our results demonstrate that the Cu-BTC/MOF modified with the NO₂ group has a good adsorption effect on Rh B, which has practical reference significance for medical wastewater and the actual treatment of printing and dyeing wastewater in the future.

Table 2. The different MOFs/dye systems used in our study.

Systems	Adsorbent	No. of Rh B	No. Water molecules	No. Na ⁺	No. Cl ⁻	Simulation box size (nm ³)
MOF-Rh B	Cu-BTC/MOF	10	12,074	34	45	8*8*6
MOF-NH ₂	Cu-BTC/MOF-NH ₂	10	11,995	34	45	8*8*6
MOF-OH	Cu-BTC/MOF-OH	10	12,029	34	45	8*8*6
MOF-NO ₂	Cu-BTC/MOF-NO ₂	10	11,974	34	45	8*8*6

METHODS

The crystal structure of Cu-BTC/MOF, the model adsorbent, is taken from the Chemtub3D website, and its initial atomic charges are taken from the Zhao group⁴³. Furthermore, the structural data file for Rhodamine B (PubChem CID: 6694) molecule is obtained from the PubChem database (Supplementary Fig. 2). Four simulation boxes called MOF-Rh B, MOF-NH₂, MOF-OH, and MOF-NO₂ are designed, which all contained an adsorbent and ten Rh B molecules (See Supplementary Fig. 3). For construction of the F-MOF systems, all the hydrogen atoms in the Cu-BTC/MOF organic linker part are replaced by NH₂, OH, and NO₂ groups. The Cu-BTC/MOF unit cell and functional groups used in this work are represented in Fig. 9a, b. More information about designed systems is provided in Table 2. The CHARMM36 force field is used to obtain the force field parameters for the dye molecule and adsorbents⁴⁴. All four systems are neutralized and solvated with the NaCl ions and TIP3P water model, respectively⁴⁵. The V-rescale thermostat is applied for temperature control at 310 K, and pressure is stabilized at 1 atm using the Berendsen aerostat^{46,47}. LINCS algorithm is regarded to constrain bond lengths of all the bonds at their equilibrium position⁴⁸. Long-range electrostatic interactions are accounted for using the Particle Mesh Ewald procedure^{47,49}, while periodic boundary conditions are imposed with a 1.4 nm cutoff for nonbonded interactions. The Visual Molecular Dynamics graphics software is employed for visualizing molecules^{47,50}. Well-tempered metadynamics simulations are employed to obtain FE surfaces⁵¹. The WT-MtD simulation has been performed for 75 ns after the equilibration utilizing the PLUMED version 2.5.2 plugin to the Gromacs 2019.2 software^{52,53}. The FE surface is computed as a function of the distance between the center of mass (COM) of Rh B and the adsorbent surface and between Rh B's COM and functional groups. More details concerning the WT-MtD simulations are provided in the "Results and discussion" Section "METADYNAMICS".

DATA AVAILABILITY

Authors can confirm that all relevant data are included in the article and/or its supplementary information files

CODE AVAILABILITY

The codes that support the findings of this study are available from the corresponding authors upon reasonable request.

Received: 29 April 2022; Accepted: 13 September 2022;

Published online: 22 September 2022

REFERENCES

- Wu, J. et al. Plasma modification of Fe-MOF for efficient organic pollutants removal. *J. Solid State Chem.* **302**, 122350 (2021).
- Routoula, E. & Patwardhan, S. V. Degradation of anthraquinone dyes from effluents: a review focusing on enzymatic dye degradation with industrial potential. *J. Environ. Sci.* **54**, 647–664 (2020).
- Steplin Paul Selvin, S. et al. Photocatalytic degradation of rhodamine B using zinc oxide activated charcoal polyaniline nanocomposite and its survival assessment using aquatic animal model. *ACS Sustain. Chem. Eng.* **6**, 258–267 (2018).
- Saleh, T. A., Tuzen, M. & Sari, A. Evaluation of poly (ethylene diamine-trimesoyl chloride)-modified diatomite as efficient adsorbent for removal of rhodamine B from wastewater samples. *Environ. Sci. Pollut.* **28**, 55655–55666 (2021).
- Yuan, S., Fan, Y., Zhang, Y., Tong, M. & Liao, P. Pd-catalytic in situ generation of H₂O₂ from H₂ and O₂ produced by water electrolysis for the efficient electro-Fenton degradation of rhodamine B. *Environ. Sci. Technol.* **45**, 8514–8520 (2011).
- Borthakur, P. et al. Experimental and molecular dynamics simulation study of specific ion effect on the graphene oxide surface and investigation of the influence on reactive extraction of model dye molecule at water organic interface. *J. Phys. Chem. C* **120**, 14088–14100 (2016).
- Ayati, A., Shahrak, M. N., Tanhaei, B. & Sillanpää, M. Emerging adsorptive removal of azo dye by metal-organic frameworks. *Chemosphere* **160**, 30–44 (2016).
- Assaf, M., Martin-Gassin, G., Prelot, B. & Gassin, P.-M. Driving forces of cationic dye adsorption, confinement, and long-range correlation in zeolitic materials. *Langmuir* **38**, 1296–1303 (2022).
- Pachisia, S., Gupta, R. & Gupta, R. Molecular assemblies offering hydrogen-bonding cavities: influence of macrocyclic cavity and hydrogen bonding on dye adsorption. *Inorg. Chem.* **61**, 3616–3630 (2022).
- Zhao, P. et al. A new paradigm of ultrathin 2D nanomaterial adsorbents in aqueous media: graphene and GO, MoS₂, MXenes, and 2D MOFs. *J. Mater. Chem.* **7**, 16598–16621 (2019).
- Narayanaswamy, V. et al. Adsorption of methylene blue and rhodamine B on graphene oxide-Fe₃O₄ nanocomposite: Molecular dynamics and Monte Carlo simulations. *Mater* **10**, 314–324 (2020).
- Pastore, V. J., Cook, T. R. & Rzayev, J. Polymer-MOF hybrid composites with high porosity and stability through surface-selective ligand exchange. *Chem. Mater.* **30**, 8639–8649 (2018).
- Yan, Y. et al. Facile immobilization of ethylenediamine tetramethylene-phosphonic acid into UiO-66 for toxic divalent heavy metal ions removal: An experimental and theoretical exploration. *Sci. Total Environ.* **806**, 150652 (2022).
- Matheu, R. et al. Three-dimensional phthalocyanine metal-catecholates for high electrochemical carbon dioxide reduction. *J. Am. Chem. Soc.* **141**, 17081–17085 (2019).
- Fuchs, A. et al. Single crystals heterogeneity impacts the intrinsic and extrinsic properties of metal organic frameworks. *Adv* **34**, 2104530 (2022).
- Gordon, J., Kazemian, H. & Rohani, S. MIL-53 (Fe), MIL-101, and SBA-15 porous materials: potential platforms for drug delivery. *Mater. Sci. Eng. C* **47**, 172–179 (2015).
- Firouzjaei, M. D., Afkhami, F. A., Esfahani, M. R., Turner, C. H. & Nejati, S. Experimental and molecular dynamics study on dye removal from water by a graphene oxide-copper-metal organic framework nanocomposite. *J. Water Process. Eng.* **34**, 101180 (2020).
- Chowdhury, P., Bikkina, C. & Gumma, S. Gas adsorption properties of the chromium-based metal organic framework MIL-101. *J. Phys. Chem. C* **113**, 6616–6621 (2009).
- Li, J.-R., Sculley, J. & Zhou, H.-C. Metal-organic frameworks for separations. *Chem* **112**, 869–932 (2012).
- Sadati, A. K. et al. A qualitative study on stigmatization associated with COVID-19. *Prim. Care Companion CNS Disord.* **24**, 40320 (2022).
- Achmann, S. et al. Sulfur removal from low-sulfur gasoline and diesel fuel by metal-organic frameworks. *Chem. Eng. Technol. Ind. Chem.-Plant Equip.-Process Eng.-Biotechnol.* **33**, 275–280 (2010).
- Cychosz, K. A. & Matzger, A. J. Water stability of microporous coordination polymers and the adsorption of pharmaceuticals from water. *Langmuir* **26**, 17198–17202 (2010).
- Maes, M., Vermoortele, F., Alaerts, L., Denayer, J. F. M., & De Vos, D. E. Separating saturated alkyaromatics from their unsaturated analogues using metal-organic frameworks. *J. Phys. Chem. C* **115**, 1051–1055 (2011).
- Haque, E., Jun, J. W. & Jhung, S. H. Adsorptive removal of methyl orange and methylene blue from aqueous solution with a metal-organic framework material, iron terephthalate (MOF-235). *J. Hazard. Mater.* **185**, 507–511 (2011).

25. Gong, R. et al. Adsorptive removal of methyl orange and methylene blue from aqueous solution with finger-citron-residue-based activated carbon. *Ind. Eng. Chem. Res.* **52**, 14297–14303 (2013).
26. Koutahzadeh, N., Esfahani, M. R., Bailey, F., Taylor, A. & Esfahani, A. R. Enhanced performance of polyhedral oligomeric silsesquioxanes polysulfone nanocomposite membrane with improved permeability and antifouling properties for water treatment. *J. Environ. Chem. Eng.* **6**, 5683–5692 (2018).
27. Horiuchi, Y. et al. Visible-light-promoted photocatalytic hydrogen production by using an amino-functionalized Ti (IV) metal–organic framework. *J. Phys. Chem. C* **116**, 20848–20853 (2012).
28. Lin, W., Rieter, W. J. & Taylor, K. M. L. Modular synthesis of functional nanoscale coordination polymers. *Angew. Chem. Int. Ed.* **48**, 650–658 (2009).
29. Hollingsworth, S. A. & Dror, R. O. Molecular dynamics simulation for all. *Neuron* **99**, 1129–1143 (2018).
30. Buglak, A. A., Samokhvalov, A. V., Zherdev, A. V. & Dzantiev, B. B. Methods and applications of in silico aptamer design and modeling. *Int. J. Mol. Sci.* **21**, 8420 (2020).
31. Cao, Y. et al. Molecular dynamic simulations and quantum chemical calculations of adsorption process using amino-functionalized silica. *J. Mol. Liq.* **330**, 115544 (2021).
32. Shadrack, D. M. & Swai, H. S. Solvent effects on molecular encapsulation of Toussantine-A by chitosan nanoparticle: A metadynamics study. *J. Mol. Liq.* **292**, 111434 (2019).
33. Mantasha, I. et al. Efficient and selective adsorption and separation of methylene blue (MB) from mixture of dyes in aqueous environment employing a Cu (II) based metal organic framework. *Inorg. Chim. Acta* **511**, 119787 (2020).
34. Chang, S., Zhang, Q., Lu, Y., Wu, S. & Wang, W. High-efficiency and selective adsorption of organic pollutants by magnetic CoFe₂O₄/graphene oxide adsorbents: Experimental and molecular dynamics simulation study. *Sep. Purif. Technol.* **238**, 116400 (2020).
35. Narayanaswamy, V. et al. Molecular simulation of adsorption of methylene blue and rhodamine B on graphene and graphene oxide for water purification. *Mater. Today: Proc.* **28**, 1078–1083 (2020).
36. Ahamad, M. N., Khan, M. S., Shahid, M. & Ahmad, M. Metal organic frameworks decorated with free carboxylic acid groups: topology, metal capture and dye adsorption properties. *Dalton Trans.* **49**, 14690–14705 (2020).
37. Qin, W., Li, X., Bian, W.-W., Fan, X.-J. & Qi, J.-Y. Density functional theory calculations and molecular dynamics simulations of the adsorption of biomolecules on graphene surfaces. *Biomaterials* **31**, 1007–1016 (2010).
38. Giona, M., Cerbelli, S. & Roman, H. E. Fractional diffusion equation and relaxation in complex viscoelastic materials. *Phys. A* **191**, 449–453 (1992).
39. Kong, L., Dong, K., Tang, Y. & Lai, S. Molecular dynamics simulation of the influence of PEG-TDI aging degradation on diffusibility and compatibility of NG and BTTN. *Propellants Explos. Pyrotech.* **46**, 1436–1446 (2021).
40. Sanborn, M. J. & Snurr, R. Q. Diffusion of binary mixtures of CF₄ and n-alkanes in faujasite. *ep. Purif. Technol.* **20**, 1–13 (2000).
41. Benkhaya, S. et al. Polysulfone Polyetherimide Ultrafiltration composite membranes constructed on a three-component Nylon-fiberglass-Nylon support for azo dyes removal: Experimental and molecular dynamics simulations. *Colloids Surf. A: Physicochem. Eng. Asp.* **625**, 126941 (2021).
42. Reddy, T. D. N. & Mallik, B. S. Hydrogen bond kinetics, ionic dynamics, and voids in the binary mixtures of protic ionic liquids with alkanolamines. *J. Phys. Chem. B* **125**, 5587–5600 (2021).
43. Zhao, L. et al. A force field for dynamic Cu-BTC metal-organic framework. *J. Mol. Model* **17**, 227–234 (2011).
44. Vaiana, A. C. et al. Fluorescence quenching of dyes by tryptophan: interactions at atomic detail from combination of experiment and computer simulation. *J. Am. Chem. Soc.* **125**, 14564–14572 (2003).
45. Razavi, L., Raissi, H. & Farzad, F. Assessment of the effect of external and internal triggers on adsorption and release of paclitaxel from the PEI functionalized silicene nanosheet: A molecular dynamic simulation. *J. Mol. Graph. Model.* **106**, 107930 (2021).
46. Liu, H. & Pei, Y. Atomistic molecular dynamics simulation study on the interaction between atomically precise thiolate-protected gold nanoclusters and phospholipid membranes. *Langmuir* **38**, 1653–1661 (2022).
47. Kobierski, J. et al. How the replacement of cholesterol by 25-hydroxycholesterol affects the interactions with sphingolipids: The Langmuir Monolayer Study complemented with theoretical calculations. *J. R. Soc. Interface* **18**, 20210050 (2021).
48. Thallmair, S., Javanainen, M., Fábíán, B., Martínez-Seara, H. & Marrink, S. J. Non-converged constraints cause artificial temperature gradients in lipid bilayer simulations. *J. Phys. Chem. B* **125**, 9537–9546 (2021).
49. Shobhna & Kashyap, H. K. Deciphering ethanol-driven swelling, rupturing, aggregation, and fusion of lipid vesicles using coarse-grained molecular dynamics simulations. *Langmuir* **38**, 2445–2459 (2022).
50. Vatanpour, V. et al. Hyperbranched polyethylenimine functionalized silica/poly-sulfone nanocomposite membranes for water purification. *Chemosphere* **290**, 133363 (2022).
51. Chrobak, W. et al. Component of cannabis, cannabidiol, as a possible drug against the cytotoxicity of A β (31-35) and A β (25-35) peptides: an investigation by molecular dynamics and well-tempered metadynamics simulations. *ACS Chem. Neurosci.* **12**, 660–674 (2021).
52. Wang, D. et al. Efficient sampling of high-dimensional free energy landscapes using adaptive reinforced dynamics. *Nat. Comput. Sci.* **2**, 20–29 (2022).
53. Carvalho Martins, L., Cino, E. A. & Ferreira, R. S. PyAutoFEP: an automated free energy perturbation workflow for GROMACS integrating enhanced sampling methods. *J. Chem. Theory Comput.* **17**, 4262–4273 (2021).

AUTHOR CONTRIBUTIONS

L.R.: Writing - Design simulation systems. H.R.: Supervision, Writing - review & editing. H.H.: review & editing. F.F.: review & editing.

COMPETING INTERESTS

The authors declare no competing interests.

ADDITIONAL INFORMATION

Supplementary information The online version contains supplementary material available at <https://doi.org/10.1038/s41545-022-00195-w>.

Correspondence and requests for materials should be addressed to Heidar Raissi.

Reprints and permission information is available at <http://www.nature.com/reprints>

Publisher's note Springer Nature remains neutral with regard to jurisdictional claims in published maps and institutional affiliations.



Open Access This article is licensed under a Creative Commons Attribution 4.0 International License, which permits use, sharing, adaptation, distribution and reproduction in any medium or format, as long as you give appropriate credit to the original author(s) and the source, provide a link to the Creative Commons license, and indicate if changes were made. The images or other third party material in this article are included in the article's Creative Commons license, unless indicated otherwise in a credit line to the material. If material is not included in the article's Creative Commons license and your intended use is not permitted by statutory regulation or exceeds the permitted use, you will need to obtain permission directly from the copyright holder. To view a copy of this license, visit <http://creativecommons.org/licenses/by/4.0/>.

© The Author(s) 2022